Available online at www.sciencedirect.com
SCIENCE DIRECT
Fuel 84 (2005) 2116–2130
FUEL
www.fuelfirst.com

Effect of fuel properties on biomass combustion. Part II. Modelling approach—identification of the controlling factors

Yao Bin Yang[a,*], Changkook Ryu[a], Adela Khor[a], Nicola E. Yates[b], Vida N. Sharifi[a], Jim Swithenbank[a]

[a]*Sheffield University Waste Incineration Centre (SUWIC), Department of Chemical and Process Engineering, Sheffield University, Mappin Street, Sheffield S1 3JD, UK*
[b]*Rothamsted Research, Harpenden, Herts AL5 2JQ, UK*

Received 8 March 2005; received in revised form 22 April 2005; accepted 26 April 2005
Available online 13 June 2005

Abstract

Biomass fuels come from many varieties of sources resulting in a wide range of physical and chemical properties. In this work, mathematical models of a packed bed system were employed to simulate the effects of four fuel properties on the burning characteristics in terms of burning rate, combustion stoichiometry, flue gas composition and solid-phase temperature. Numerical calculations were carried out and results were compared with measurements wherever possible. It was found that burning rate is mostly influenced by fuel size and smaller fuels result in higher combustion rate due to increased reacting surface area and enhanced gas-phase mixing in the bed; combustion stoichiometry is equally influenced by fuel LCV and size as a consequence of variation in burning rate as well as the mass ratio of combustible elements to the oxygen in the fuel; for the solid-phase temperature, material density has the strongest influence and a denser material has a higher maximum bed temperature as it results in a less fuel-rich combustion condition; while CO concentration in the flue gases is mostly affected by both fuel calorific value and size, CH_4 in the exiting flow is greatly affected by material density due to change in reaction zone thickness.

Keywords: Biomass; Combustion; Mathematical modelling

1. Introduction

Biomass constitutes 14% of the global primary energy, the fourth largest following coal, oil and natural gas. It is renewable and produces no net CO_2 emission in combustion. Fuel biomass comes from both primary and secondary sources. Primary sources are energy crops that have the sole purpose of energy production. Willow, miscanthus, reed canary grass and sorghum are a few examples of this category. Secondary sources are mainly from agriculture activities and wastes, including straw, forest residues, sugar cane fibre, rice husks, waste vegetables, cardboard and paper, etc.

The wide variety of biomass sources result in a wide range of biomass fuel properties, both physically and chemically. Table 1 illustrates the estimated variations of conventional properties of biomass which can be measured by standard methods. Moisture, for instance, can only be a few percent with pre-dried biomass or as high as 50% with freshly harvested crops. Volatile matter in biomass is much higher than in coals, ranging from 65 to 85%, while fixed carbon is much lower, ranging from 7 to 20%. Ash is generally under 5%, but can be as high as 20% with some specific mass, for example, rice hulls. For elemental analysis, a noticeable feature is the high oxygen content (32–45%).

Depending on the type of species and specific cultivation conditions, levels of other minor components, such as N, S, Cl and K can also vary widely.

The lower calorific value (LCV) ranges from 15 to 22 MJ kg^{-1} and the size can be from that of pulverized particles ($\sim$1 mm) to that of whole wood logs ($\sim$100 mm).

* Corresponding author. Tel.: +44 114 2227500; fax: +44 114 2227501.
E-mail address: y.b.yang@shef.ac.uk (Y.B. Yang).

0016-2361/$ - see front matter © 2005 Elsevier Ltd. All rights reserved.
doi:10.1016/j.fuel.2005.04.023

Nomenclature

A	flow cross-section area, m^2; particle surface area, $m^2\ m^{-3}$
A_r	pre-exponent factor in char burning rate, kg $m^{-2}\ s^{-1}$
A_v	pre-exponent factor in devolatilisation rate, s^{-1}
Bi	Biot number
Bi′	modified Biot number
C	constant; molar fractions of species
C_{fuel}	fuel concentration, kg m^{-3}
C_{pg}	specific heat capacity of the gas mixture, J $kg^{-1}\ K^{-1}$
C_{mix}	mixing-rate constant, 0.5
$C_{w,g}$	moisture mass fraction in the gas phase
$C_{w,s}$	moisture mass fraction at the solid surface
D_g	molecular diffusion coefficient of volatile hydrocarbons in air, $m^2\ s^{-1}$
D_{ig}	dispersion coefficients of the species Y_i, $m^2\ s^{-1}$
d_p	particle diameter, m
E_b	black body emission, Wm^{-2}
E_r	activation energy in char burning rate, J $kmol^{-1}$
E_v	activation energy in devolatilization rate, J $kmol^{-1}$
E^0	effective diffusion coefficient
F_2	fraction of the volume occupied by water replaced by pores during drying
F_3	fraction of the volume occupied by volatile matter replaced by pores during pyrolysis
FC	fixed carbon in fuel, wt%
H_{evp}	evaporation heat of the solid material, J kg^{-1}
H_g	gas enthalpy, J kg^{-1}
H_s	solid-phase enthalpy, J kg^{-1}
h_s	convective mass transfer coefficient between solid and gas, kg $m^{-2}\ s^{-1}$
h'_s	convective heat transfer coefficient between solid and gas, W $m^{-2}\ K^{-1}$
I_x^+	radiation flux in positive x-direction, W m^{-2}
I_x^-	radiation flux in negative x-direction, W m^{-2}
k	thermal conductivity of particle material, W $m^{-1}\ K^{-1}$
k_a	radiation absorption coefficient, m^{-1}
k_d	rate constants of char burning due to diffusion, kg $m^{-2}\ s^{-1}$
k_r	rate constants of char burning due to chemical kinetics, kg $m^{-2}\ s^{-1}$
k_v	rate constant of devolatilization, s^{-1}
k_s	radiation scattering coefficient, m^{-1}
K	permeability
L_b	bed top height, m
M	moisture in fuel, wt%
PA_i	primary air velocity levels ($i=1,4$)
p_g	gas pressure, Pa
Q_h	heat loss/gain of the gases, W m^{-3}
Q_{sh}	thermal source term for solid phase, W m^{-3}
q_r	radiative heat flux, W m^{-2}
R_i	process rate ($i=2,3,4$), kg $m^{-3}\ s^{-1}$
R	Universal gas constant; reaction rate
R_{mix}	mixing-rate of gaseous phase in the bed, kg $m^{-3}\ s^{-1}$
S	stoichiometric coefficients in reactions
S_{sg}	conversion rate from solid to gases due to evaporation, devolatilisation and char burning, kg $m^{-3}\ s^{-1}$
Sy_{ig}	mass sources due to evaporation, devolatilisation and combustion, kg $m^{-3}\ s^{-1}$
Sy_{is}	source term, kg $m^{-3}\ s^{-1}$
t	time instant, s
T	temperature, K
V	velocity, ms^{-1}; volume of the bed, m^3
V_0	volume of the initial bed, m^3
VM	volatile matter in fuel, wt%
x	co-ordinate in bed height direction, m
Y_{ig}	mass fractions of individual species (e.g. H_2, H_2O, CO, CO2, C_mH_n,…).
Y_{is}	mass fractions of particle compositions (moisture, volatile, fixed carbon and ash)
$Y_{is,0}$	mass fraction of particles components at fresh feed state;
ε_s	system emissivity
σ_b	Stefan–Boltzmann constant, 5.86×10^{-8} W $m^{-2}\ K^{-4}$
υ	remaining volatile in solid at time t
υ_∞	ultimate yield of volatile
ϕ	void fraction in the bed
ρ	density, kg m^{-3}
ρ_{sb}	solid bulk density in the bed, kg m^{-3}
λ_g	thermal dispersion coefficient, W $m^{-1}\ K^{-1}$
λ_g^0	effective thermal diffusion coefficient, W $m^{-1}\ K^{-1}$
λ_s	effective thermal conductivity of the solid bed, W $m^{-1}\ K^{-1}$
μ	viscosity of gases, kg $m^{-1}\ s^{-1}$
$\omega_{i,k}$	volume fraction of component i in biomass k

Subscripts

env	environmental
g	gas phase
i	identifier for a component in the solid
p	particle
s	solid phase
2	moisture or moisture evaporation
3	volatile matter or devolatilisation
4	fixed carbon or char gasification
A	material in its initial state
B	dried material
C	dried and pyrolysed material
D	dried, pyrolysed and gasified material

Table 1
Variations in biomass fuel properties

M	VM	FC	Ash	C	H	O	N	S
5–50	65–85	7–20	0.5–20	38–53	4.5–7.0	32–45	0.15–2.7	0.02–0.35
Cl	LCV, MJ kg^{-1}	d_p, mm	Maximum dimension ratio		Thermal conductivity, k_s		Bulk density, ρ_{sb}	
0–0.5	15–22	1–100	1–15		0.07–0.5 W m^{-1} K^{-1}		20–710 kg m^{-3}	

The unit of the properties is in wt% unless indicated otherwise; elemental composition is on a dry basis.

The shape is non-spherical, normally with high dimension ratios and some biomass is pelletised to form a single shape and size. Bulk density of biomass fuels vary significantly, from the very light dry straw (20 kg m^{-3}) to the very heavy pellets ($\sim$700 kg m^{-3}).

This wide variation in biomass properties can greatly affect the burning characteristics of the biomass fuels. The effect of moisture level in fuel for packed bed systems was investigated by Yang et al. [1,2] in conjunction with primary air velocity in a packed bed. It was found that the maximum burning rate with a very dry fuel can be several times higher than with a very wet fuel and the reaction zone thickness becomes thinner as the moisture level in fuel increases. Flame extinction also occurs at high moisture levels, which was related to the minimum amount of combustible material (both volatile in solids and char) above the moisture evaporation layer. Thunman & Leckner [3] presented a calculated maximum propagation rate of the reaction front for 10 mm wood particles with different moisture contents. They also quoted the experimental results of Gort [4] with moisture level in fuel ranging from 10 to 56.6% on a wet basis.

Yang et al. [5] studied the effect of devolatilisation rate on biomass combustion characteristics in a packed bed which shows that the devolatilisation rate has an increasing influence as the moisture content in fuel decreases.

Some effects of the physical properties of biomass were also investigated though the conclusions were inconsistent. For example, Gort [4] and Rönnbäck et al. [6] reported increased ignition speed for larger particles in the size range of 10–30 mm while Peters [7] reported the maximum ignition rate was obtained at 15 mm in the size range of 5–25 mm. On the other hand, Friberg and Blasiak [8] demonstrated decreasing burning rate as particles size increased.

The effect of biomass fuel properties also depends on the type of reacting systems. There are three major types of reactor for biomass combustion: packed-bed, fluidized bed and entrained flow reactors. The packed-bed system is the mostly widely used, from small-scale home application to large-scale industrial facilities. The advantages of the system are minimum fuel pre-treatment, relatively well-known technology and low construction and running costs.

Overall, detailed and systemic studies on the effect of fuel properties on biomass combustion are still lacking, while demand for more information is increasing as more and more efforts are being made to utilize effectively and environmentally friendly the global biomass resources. Experimental approaches, though, provide invaluable practical data, however isolating one parameter from the rest with experimental methods is difficult to implement. The bulk density of the materials, for example, is very difficult to change unless the fuel is pelletised. Often the fuel sample comes with a specific particle size (or size distribution), bulk density and fixed contents of volatile matter, fixed carbon and ash. The sample may be pretreated by drying or wetting to vary moisture content, but nothing more can be done with the sample. This put a limitation to the experimental approach when the effect of individual parameters needs to be addressed.

Mathematical modeling, on the other hand, provides a flexible approach to evaluate the effects of individual fuel properties. The volatile content, for example, can be varied artificially, so can the particle size and its distribution, provided that the mathematical models incorporate those physical and chemical parameters. Mathematical modeling also provides such detailed information as temperature profile, gas compositions, bed height decrease, pollutant formation and combustion stoichiometry, etc.

In this paper, the mathematical approach is adopted to identify the controlling factors during biomass combustion in packed bed systems. The effects of fuel LCV, material density, particle size and packed bed porosity are investigated. The results from mathematical calculations are compared to experimental measurements where it is possible. Extensive numerical calculations are carried out in wide ranges of fuel parameters, and the results are presented in terms of average burning rate, combustion stoichiometry, bed temperature and gas compositions at the bed top. Experimental work is introduced in Part I of this paper.

2. Mathematical description of packed-bed biomass combustion

Peters [7] proposed the governing equations for packed-bed solid combustion. Yang et al. [9] first applied the proposed equations to waste incineration in a moving grate, followed by a series of theoretical studies on the effect of fuel moisture, devolatilisation rate and primary air velocity [1,2,5].

A packed bed consists of a number of solid particles which are piled up upon a support grate with a characteristic porosity. Primary air is supplied from underneath the grate and flows upward. For ordinary packed bed combustion, ignition starts at the bed top layer heated up by over-bed radiation from the over-bed flame and hot walls. Once the bed is ignited, the flame front travels downwards at a speed depending on fuel type and operating parameters, until it arrives at the bed bottom or the support grate. In ideal conditions, three reacting waves travel down the bed successively: moisture evaporation, devolatilisation and char combustion (Fig. 1). They may overlap each other, depending upon particle size or the Biot number. The Biot number is a measure of uniformity of temperature distribution inside a particle and for a single particle heated uniformly at the external surface, it is defined as

$$\mathrm{Bi} = h'_s d_p / k \tag{1}$$

When $\mathrm{Bi} \gg 1.0$ particles are considered thermally thick and there exists a significant temperature gradient inside the particles under an external heating source. Otherwise, the particles can be viewed as thermally thin, and the temperature gradient inside the particle is small.

The above definition of Biot number for a single particle, however, has to be modified to account for the changed heating conditions for the situation of a packed bed. Radiation from the flame front can only penetrate the bed through voids; therefore the actual external heated area of a particle in a packed bed is proportional to the local bed voidage. So we add an extra parameter, the void fraction to the original Biot number and the modified Biot Number is thus as follows:

$$\mathrm{Bi}' = \phi h'_s d_p / k \tag{1a}$$

Assuming an external radiation source of 1100 K, a bed porosity of 0.5 and the thermal conductivity of the particles being $k = 0.4\ \mathrm{W\ m^{-1}\ K^{-1}}$ [10], the modified Biot number $\mathrm{Bi}' < 1$ when $d_p < 15$ mm and $\mathrm{Bi}' < 2$ when $d_p < 30$ mm. So, generally speaking, particles smaller than 30 mm can be roughly regarded as thermally thin in the situation of packed bed combustion.

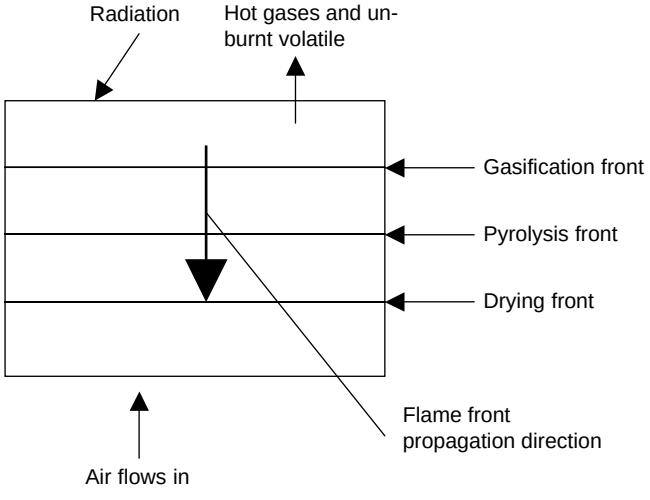

Fig. 1. Propagation of flame front in a packed bed.

The assumption of thermally thin particles eliminates the need for a separate solution for temperature profile inside the particles. Instead, the whole bed can be viewed as a continuous porous medium with two phases (solid and gases), and continuous conservation or transport equations can be applied to both phases in a much simpler way. Table 2 summarises the equations employed for packed-bed biomass combustion in this work.

The whole set of equations consists of bed volume change, individual process rates, gaseous phase and solid phase conservation equations and radiation heat transfer in the bed. Biomass particles shrink as they lose mass through moisture evaporation, volatile release and char burnout and so the bed volume decreases as a result. Change in the bed volume is related to each individual process rates, R_2 for moisture evaporation, R_3 for devolatilisation and R_4 for char burnout. Moisture in the fuel evaporates via two mechanisms, convective drying by primary air and radiative drying by radiation from the flame front. For biomass devolatilisation, a single step global reaction proposed by Badzioch et al. [11] is adopted for simplicity. The pre-exponential factor A_v and activation energy E_v are fixed at $7.0 \times 10^4\ \mathrm{s^{-1}}$ and $83\ \mathrm{kJ\ mol^{-1}}$, respectively [12].

The gaseous products of devolatilisation are C_mH_n, CO, CO_2, H_2O and H_2 (C_mH_n is taken as CH_4 in this study). The two-step reaction mechanism is assumed for the oxidation of C_mH_n with CO and H_2 as the intermediate products. The gas-phase burning of C_mH_n, CO and H_2 is not only controlled by the kinetic rate but also by the mixing rate of the released volatile gases with primary air flow coming from underneath the grate. The gas-phase mixing rate is modeled by an equation proposed by Yang et al. [9] which relates the mixing rate to particle size, bed voidage and gas velocity. The actual burning rate of the combustible volatile gases is taken as the minimum of the kinetic rate and mixing rate.

The char formed from the devolatilisation process reacts with oxygen in the primary air flow to form both CO and CO_2, with the ratio of CO to CO_2 determined by the temperature level. The gasification rate of char is controlled by both the kinetic rate and the diffusion rate. The parameters in the kinetic rate, k_r, are taken as $A_r = 290\ \mathrm{kg\ m^{-2}\ s^{-1}}$ and $E_r = 86\ \mathrm{kJ\ mol^{-1}}$ [13].

The conservation equations for the gas-phase in the packed bed include continuity, momentum, species and energy conservation equations. The gas species include O_2, CO_2, CO, H_2, CH_4, H_2O balanced by N_2. The conservation equations for the solid-phase take forms similar to the gas-phase, and the radiation heat transfer in the bed is modeled by the two-flux model proposed initially by Gosman & Lockwood [14].

Table 2
Summary of the equations employed for packed-bed biomass combustion

			Reference
Bed volume change		$\frac{dV}{V_0\,dt}=\frac{R_2}{\rho_2\omega_{2,A}}\left[\frac{(\phi_B-\phi_A)-(1-\phi_A)(1-F_2)\omega_{2,A}}{(1-\phi_B)(1-\phi_A)}\right]+\frac{R_3}{\rho_3\omega_{3,B}}\left[\frac{(\phi_C-\phi_B)-(1-\phi_B)(1-F_3)\omega_{2,B}}{(1-\phi_C)(1-\phi_B)}\right]+\frac{R_4}{\rho_4\omega_{4,C}}\left[\frac{(\phi_D-\phi_C)}{(1-\phi_D)(1-\phi_C)}\right]$	Goh et al. [15]
Process rate equations	Moisture evaporation	$R_2=A_p h_s(C_{w,s}-C_{w,g})$ when $T_s<100$ °C	Goh et al. [15]
		$R_2=\frac{A_p[h'_s(T_g-T_s)+\varepsilon_s\sigma_b(T_{env}^4-T_s^4)]}{H_{evp}}$ when $T_s=100$ °C	Goh et al. [15]
	Devolatilisation	$R_3(1-\phi)\rho_s k_v(\nu_\infty-\nu)\quad k_v=A_v\exp\left(-\frac{E_v}{RT_s}\right)$	Badzioch [11]
	Combustion of volatiles	$C_mH_n+\frac{m}{2}O_2\rightarrow mCO+\frac{n}{2}H_2\quad R_{C_mH_n}=59.8T_gP^{0.3}\exp(-12200/T_g)C_{C_mH_n}^{0.5}C_{O_2}$	Siminski et al. [16]
		$CO+\frac{1}{2}O_2\rightarrow CO_2\quad R_{CO}=1.3\times10^{11}\exp(-62700/T_g)C_{CO}C_{H_2O}^{0.5}C_{O_2}^{0.5}$	Howard et al. [17]
		$H_2+\frac{1}{2}O_2\rightarrow H_2O\quad R_{H_2}=3.9\times10^{17}\exp(-20500/T_g)C_{H_2}^{0.85}C_{O_2}^{1.42}$	Hautman et al. [18]
		$R_{mix}=C_{mix}\rho_g\left[150\frac{D_g(1-\phi)^{2/3}}{d_p^2\phi}+1.75\frac{V_g(1-\phi)^{1/3}}{d_p\phi}\right]\min\left[\frac{C_{fuel}}{S_{fuel}},\frac{C_{O_2}}{S_{O_2}}\right]\quad R=\min[R_{kinetic},R_{mix}]$	Yang et al. [9]
	Char gasification	$C(s)+\alpha O_2\rightarrow2(1-\alpha)CO+(2\alpha-1)CO_2\quad\frac{CO}{CO_2}2500\exp\left(-\frac{6420}{T}\right)$	Arthur [19]
		$R_4=A_pC_{O_2}\left(\frac{1}{k_r}+\frac{1}{k_d}\right)\quad k_r=A_r\exp\left(-\frac{E_r}{RT_s}\right)$	Gray et al. [20], Field [21]
Gas phase conservation equations	Continuity	$\frac{\partial(\rho_g\phi)}{\partial t}+\frac{\partial(\rho_gV_g\phi)}{\partial x}=S_{sg}$	Peters [22]
	Momentum	$\frac{\partial(\rho_gV_g\phi)}{\partial t}+\frac{\partial(\rho_gV_gV_g\phi)}{\partial x}=-\frac{\partial p_g}{\partial x}+F(V_g)\quad F(V_g)=\begin{cases}-\frac{\propto}{\kappa}V_g, & \text{if } Re<10\\ -\frac{\propto}{K}V_g-\rho_gCV_gV_g, & \text{if } Re\geq10\end{cases}$	Peters [22]
	Species	$\frac{\partial(\rho_gY_{i,g}\phi)}{\partial t}+\frac{\partial(\rho_gV_gY_{i,g}\phi)}{\partial x}=\frac{\partial}{\partial x}\left(D_{ig}\frac{\partial(\rho_gY_{i,g}\phi)}{\partial x}\right)+S_{Y_{i,g}}$	Peters [22]
		$D_{ig}=E^0+0.5d_pV_g$	Wakao and Kaguei [23]
	Energy	$\frac{\partial(\rho_gH_g\phi)}{\partial t}\frac{\partial(\rho_gV_gH_g\phi)}{\partial x}=\frac{\partial}{\partial x}\left(\lambda_g\frac{\partial T_g}{\partial x}\right)+Q_h$	Peters [22]
		$\lambda_g=\lambda^0+0.5d_pV_g\rho_gC_{pg}$	Wakao and Kaguei [23]
Solid phase conservation equations	Continuity	$\frac{\partial((1-\phi)\rho_s)}{\partial t}+\frac{\partial((1-\phi)\rho_sV_s)}{\partial x}=-S_{sg}$	Yang et al. [5]
		$V_s=\frac{dV}{A\,dt}$	Goh et al. [15]
	Species	$\frac{\partial((1-\phi)\rho_sY_{i,s})}{\partial t}+\frac{\partial((1-\phi)\rho_sV_sY_{i,s})}{\partial x}=-S_{Y_{i,s}}$	Yang et al. [5]
	Energy	$\frac{\partial((1-\phi)\rho_sH_s)}{\partial t}+\frac{\partial((1-\phi)\rho_sV_sH_s)}{\partial x}=\frac{\partial}{\partial x}\left(\lambda_s\frac{\partial T_s}{\partial x}\right)+\frac{\partial q_r}{\partial x}Q_{sh}$	Yang et al. [1]
Radiation heat transfer		$\frac{dI_x^+}{dx}=-(k_a+k_s)I_x^++\frac{1}{2}k_aE_b+\frac{1}{2}k_s(I_x^++I_x^-)\qquad-\frac{dI_x^-}{dx}=-(k_a+k_s)I_x^-+\frac{1}{2}k_aE_b+\frac{1}{2}k_s(I_x^++I_x^-)$	Gosman & Lockwood [14]
		$k_s=0\quad k_a=-\frac{1}{d_p}\ln(\phi)$	Shin & Choi [24]

Boundary conditions:

at the bed bottom ($x=0$),

$T_g = 300$ K; $O_2 = 21$ vol%; $N_2 = 79$ vol%; $V_g = 0.1, 0.14, 0.19, 0.23$ kg m^{-2} s^{-1}; $\partial T_s/\partial x = 0$; $V_s = 0$; $\partial Y_{is}/\partial x = 0$;

at the bed top ($x=L_b$),

$\partial T_g/\partial x = 0$; $\partial Y_{ig}/\partial x = 0$; $\partial V_g/\partial x = 0$; $\partial T_s/\partial x = 0$; $\partial Y_{is}/\partial x = 0$; $\partial V_s/\partial x = 0$;

at $t=0$,

$T_g = 300$ K; $O_2 = 21$ vol%; $N2 = 79$ vol%; $V_g = 0.1, 0.14, 0.19, 0.23$ kg m^{-2} s^{-1}; $T_s = 300$ K; $V_s = 0$; $Y_{is} = Y_{is,0}$; $f = 0.35, 0.45, 0.55, 0.65, 0.75$;

The over-bed radiation source is set at 1123 K with an emissivity of 0.8. The primary air velocity and initial bed porosity take multiple values to cover the range of designated variation of operating parameters in this study.

The basic parameters used for the base or reference case are M = 7.5%, VM = 78%, FC = 12.5, ASH = 2%, C = 46.9%, H = 6.2%, O = 37.4%, LCV = 17.5 MJ kg^{-1}, d_p =

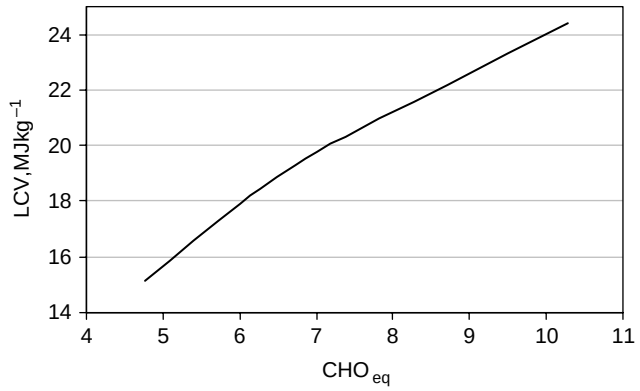

Fig. 2. Relationship between LCV and equivalence ratio of C and H to O in biomass fuel.

10 mm, $\phi = 0.65$, $\rho_{sb} = 290$ kg m^{-3} and $L_b = 410$ mm. For the variation cases, one of these parameters is varied while keeping the others the same. The four primary air levels of 0.1, 0.14, 0.19 and 0.23 kg m^{-2} s^{-1} are designated as PA1, PA2, PA3 and PA4, respectively.

The mathematical equations are solved by FLIC code developed by Yang et al. [9].

3. Results

3.1. Effect of fuel LCV

The LCV of biomass depends on the contents of moisture and ash as well as ratios of the three major elemental components, C, H and O. High moisture and high ash levels reduce the biomass LCV. Here moisture and ash in biomass are fixed at the level of the base case but the relative proportions of the three major elemental components are changed to obtain a variation in the biomass LCV. A parameter, CHO_{eq}, is used to reflect the equivalent (or stoichiometric) ratio of the combustible elements, C and H, to the non-combustible element O, based on the complete reactions of $C + O_2 = CO_2$ and $H_2 + \frac{1}{2}O_2 = H_2O$:

$$CHO_{eq} = (0.5 \times C/12 + 2.0 \times H/1.0)/(O/16) \quad (2)$$

To obtain a variation in CHO_{eq}, the ratio of C to H is fixed at the value of base case while O is varied in a certain range. The LCV of fuel is estimated as

$$LCV = 33.9\,C + 10.3\,H - 10.9\,O - 2.5 \quad (MJ\,kg^{-1}) \quad (3)$$

where the units of C, H, O and M are mass fractions.

Fig. 2 shows the relationship between LCV and the equivalence ratio of combined C and H to O in biomass fuel.

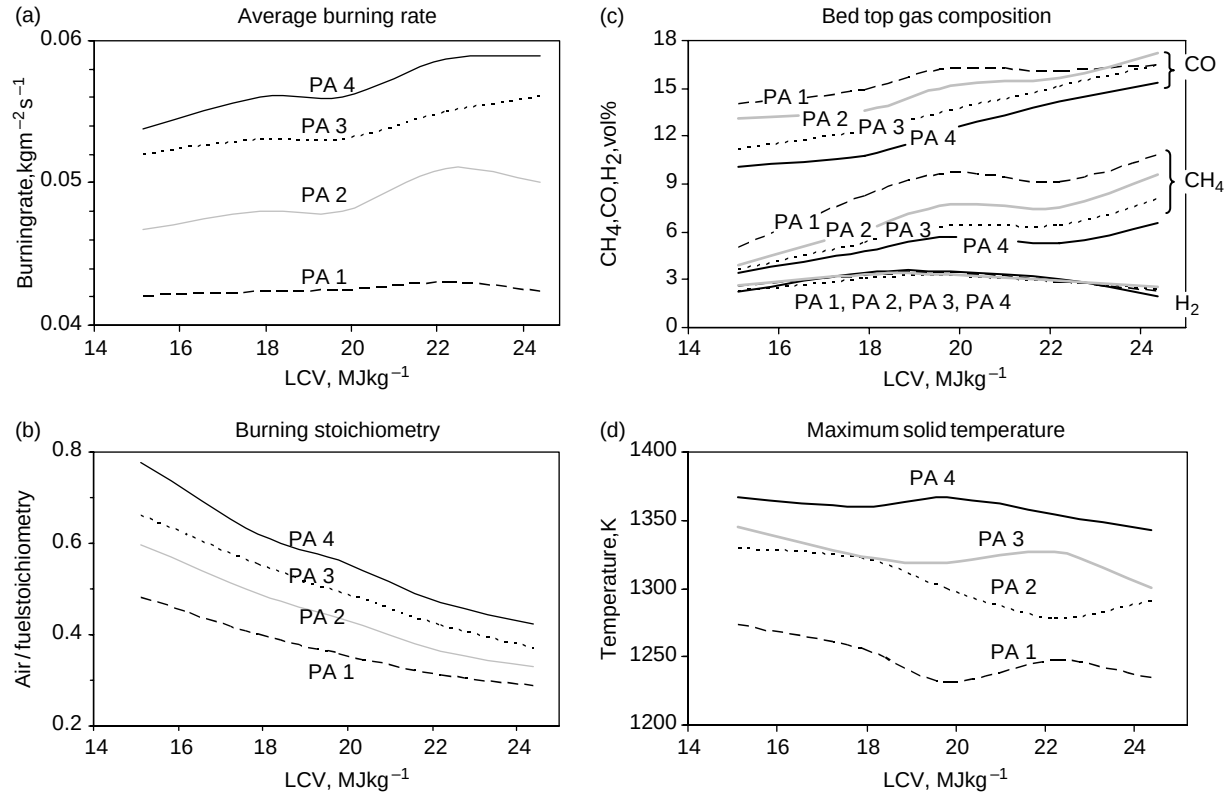

Fig. 3. Effect of fuel LCV at different primary air velocity levels: (a) average burning rate; (b) combustion stoichiometry; (c) gas composition at the bed top; (d) maximum solid temperature.

It is seen that the fuel LCV varies from 15 to 24.5 MJ kg^{-1} as CHO_{eq} covers a range from 4.8 to 10.5 and the LCV is roughly linearly proportional to the level of CHO_{eq} in fuel.

Fig. 3(a) demonstrates the calculated average burning rate vs. the fuel LCV. The average burning rate is obtained by dividing the total mass loss with the total time-span of combustion. It is seen that at a low primary air flow rate (PA1), the effect of LCV on the burning rate is quite insignificant, although the maximum is obtained around 22 MJ kg^{-1}. For a higher level of primary air flow (PA2), however, there is a slight increase in the average burning rate as LCV increases from 15 to 18 MJ kg^{-1}. The burning rate maintains virtually the same for LCV from 18 to 20 MJ kg^{-1} and then increases again for LCV from 20 to 23 MJ kg^{-1}. But for further higher LCVs, the burning rate displays a falling trend.

For the other two primary air flow levels (PA3 and PA4), the trend is similar to the situation of PA2, except that there is a continuous increase in the burning rate as the LCV rises beyond 20 MJ kg^{-1}.

Fig. 3(b) demonstrates the average air-to-fuel stoichiometric ratio as a function of LCV at the four primary airflow levels. The average value is taken over the whole time-span of combustion. The air-to-fuel stoichiometric ratio is the actual primary air supply to the packed bed compared to the theoretical air required to burn completely the combustible materials released during basically the pyrolysis process. The trend is clear: as the fuel LCV increases, the air-to-fuel stoichiometric ratio decreases and the burning process becomes more fuel-rich. At the primary air velocity level of PA1, for instance, the combustion stoichiometry drops from 0.48 to 0.28 as the LCV rises from 15 to 24.3 MJ kg^{-1}.

The burning process in a packed bed typically consists of three stages: the initial stage of ignition, the primary stage of stable combustion and the final stage of char burnout [1,5]. Fig. 3(c) shows the volumetric fractions of CH_4, CO and H_2 in the flue gases exiting the bed top during the primary stage of stable combustion, which reflects the main characteristics of biomass combustion. For CO, the general trend is increasing volume fraction as the LCV increases, especially at high levels of primary air velocity. However, at low primary air velocity (PA1), there is no noticeable change of bed-top CO level when the LCV is increased beyond 20 MJ kg^{-1}. For CH_4, the volume fraction increases initially as the LCV increases until 20 MJ kg^{-1}. Then the CH_4 level in the bed-top flue gases either remains constant at high primary air velocity (PA3 and PA4) or slightly drops at low primary air velocity (PA1 and PA2) in the range of 20–22 MJ kg^{-1}. Further increase in the LCV level, however, results in modest rise in the bed-top CH_4 level.

A quite different trend is obtained for H_2 which shows a slight variation in H_2 over the whole range of the change in LCV. The maximum is obtained at 19 MJ kg^{-1}. The primary air velocity is also found having very little influence on the H_2 level.

Fig. 3(d) presents the maximum solid temperature as a function of the fuel LCV at different primary air velocities. When the value of LCV is below 18 MJ kg^{-1}, an increase in LCV causes a fall in the maximum solid temperature (slight fall at high primary air velocity of PA4). When the LCV is greater than 18 MJ kg^{-1}, different trends are observed for different primary air velocity levels. For a low primary air velocity of PA1, as the LCV increases beyond 18 MJ kg^{-1}, a further fall in the maximum solid temperature is observed until LCV is around 20 MJ kg^{-1}, followed then by a rise and fall in the flame temperature. For the primary air velocity level of PA2, the maximum solid temperature further drops to a minimum point around 22 MJ kg^{-1}, and then rises again as the LCV increases from 18 to 24 MJ kg^{-1}. For the primary air velocity of PA3, there is not much change in the maximum solid temperature over the LCV range of 18–22 MJ kg^{-1}. But, when the LCV is increased further beyond 22 MJ kg^{-1}, the solid temperature falls; for the high primary air velocity of PA4, there is a slight fall in the maximum solid temperature as the LCV increases from 19 to 24 MJ kg^{-1}.

3.2. Effect of particle size

The particle size covered in the calculations ranges from 2 to 35 mm. Fig. 4(a) shows the burning rate as a function of particle size at different primary air velocities. Generally, larger particle size results in lower burning rate. For instance, 5 mm particles have a burning rate of 0.06 kg m^{-2} s^{-1} at a primary air velocity of PA3, which is 1.5 times of the burning rate with 30 mm particles at the same primary air velocity. One exception is for the particle sizes of 4 and 5 mm at the primary air velocity PA2 where the 5 mm particles demonstrate a higher burning rate than the 4 mm particles.

Fig. 4(b) shows the combustion stoichiometry as a function of particle size. Generally, larger-size particles result in a higher air-to-fuel stoichiometric ratio or less fuel-rich combustion. For instance, 5 mm particles have an air-to-fuel stoichiometric ratio of 0.49 at PA3 compared to the ratio being 0.74 with 30 mm particles at the same conditions. One exception is for particle sizes of 4 and 5 mm at the primary air velocities PA2 and PA3 where the 5 mm particles produce a slightly fuel-richer condition than the 4 mm particles.

Fig. 4(c) shows the bed-top gas composition as a function of particle size. For CO, the volumetric percentage ranges from around 12 to 17% and larger particles have lower CO levels at the bed top; for CH_4, the volumetric percentage ranges from 5 to 9% and a noticeable change in the relationship with the particle size is only obtained for particles smaller than 5 mm at PA1, for particles smaller than 10 mm at PA2 and for particles smaller than 15 mm at PA3. Generally, increasing particle size reduces the methane concentration at the bed top.

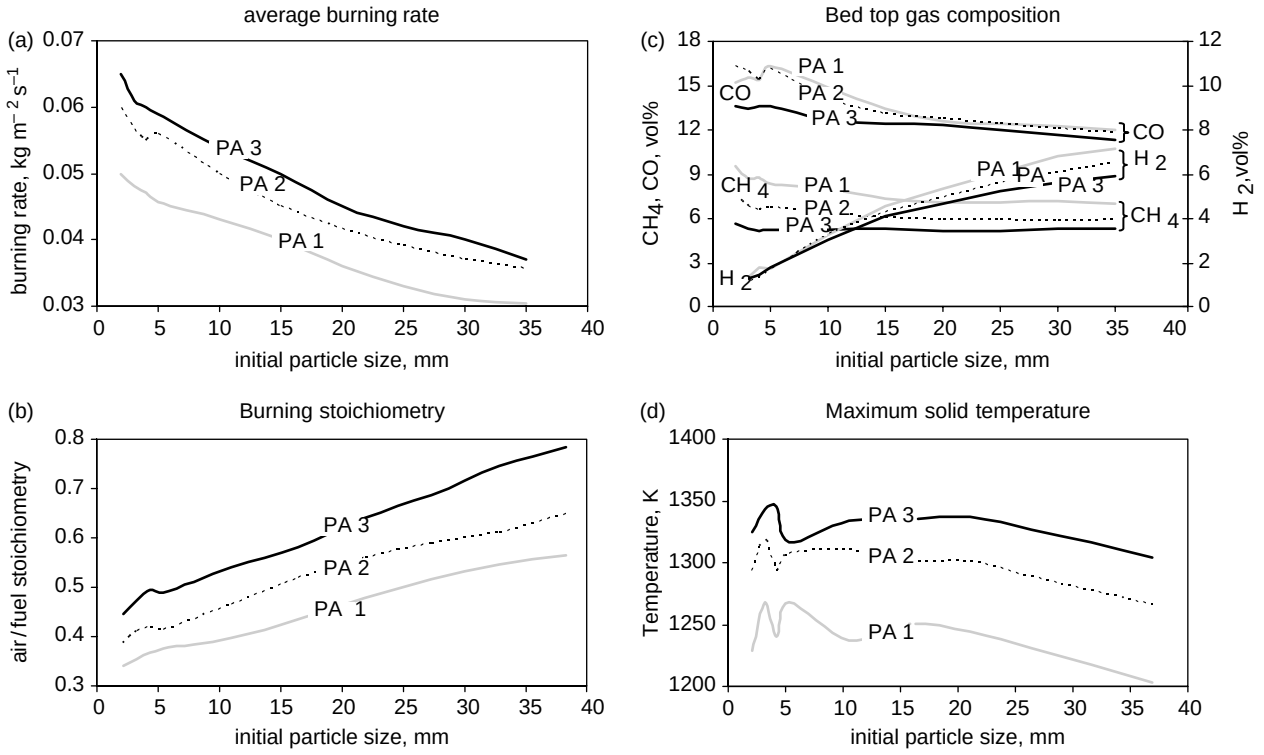

Fig. 4. Effect of particle size: (a) average burning rate; (b) combustion stoichiometry; (c) gas composition at the bed top; (d) maximum solid temperature.

For H_2, the volumetric percentage ranges from 1.5 to 7% and generally an increase in particle size results in higher hydrogen concentration at the bed top.

The primary air velocity has negligible effect on H_2 when particles are smaller than 10 mm. It also has negligible effect on CO when particle size is greater than 20 mm.

Fig. 4(d) shows the maximum solid temperature inside the bed as a function of particle size. It is seen that at PA1 the maximum solid temperature increases as particle size increases from 2 to 3 mm, then drops down 30 K at 4 mm, rises again at 5 mm to the maximum level of 1270 K. Beyond 5 mm, the general trend is decreasing solid temperature as particle size increases. At 35 mm, the maximum solid temperature is 70 K lower than the peak value obtained at 5 mm.

At PA2, the maximum solid temperature pattern in relation to the particle size is similar to the case of PA1, except that the absolute temperature level is about 50 K higher on the whole.

At PA3, the maximum solid temperature is obtained at 4 mm (1350 K) but falls to 1320 K at 5 mm. Over the range of 10–20 mm, the maximum solid temperature maintains a constant level of 1335 K.

3.3. Effect of material density

The material density covers a range from <100 to 2300 kg m^{-3}, with the light end being possibly dry straw and the heavy end, biomass pellets. Fig. 5(a) shows average burning rate as a function of biomass material density at three primary air velocity levels. At low primary air velocity (PA1), the burning rate maintains a more or less constant level between the material densities 400–800 kg m^{-3}, and then falls roughly linearly as material density rises from 800 to 1400 kg m^{-3}. The burning rate keeps constant again between densities 1400 and 1700 kg m^{-3} then falls as the material density increases further.

The situations with primary air velocities of PA1 and PA2 follow a similar pattern, with a drop in burning rate as the material density rises in the density ranges of 800–1400 kg m^{-3} and beyond 1800 kg m^{-3}. The burning rate, otherwise, remains roughly constant in relation to the material density variation.

It is also noted that material with a density of 100 kg m^{-3} produces a lower burning rate than material with a density of 200 kg m^{-3}.

Fig. 5(b) demonstrates the combustion stoichiometry as a function of material density. At low primary air velocity (PA1), the obtained air-to-fuel stoichiometric ratio ranges from 0.4 to 0.5, with a positively linear relationship between the combustion stoichiometry and the material density over the density range from 800 to 1400 kg m^{-3} and beyond 1800 kg m^{-3}. At primary air velocity levels PA2 and PA3, the pattern of change in combustion stoichiometry with increasing material density follows a similar trend to the situation of PA1, except that the whole air-to-fuel stoichiometric ratio be raised roughly 0.08 and 0.16 higher, respectively.

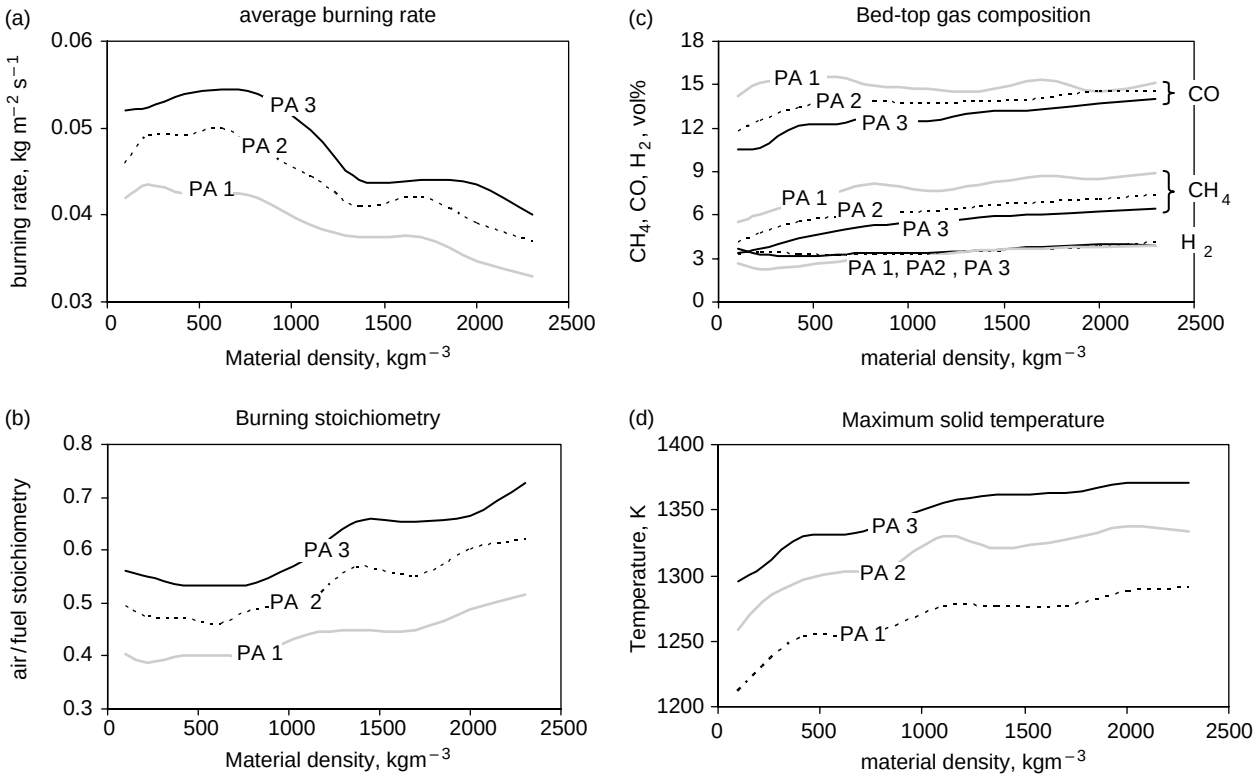

Fig. 5. Effect of material density: (a) average burning rate; (b) combustion stoichiometry; (c) gas composition at the bed top; (d) maximum solid temperature.

Fig. 5(c) shows the bed-top gas composition as a function of material density in the packed bed. For CO at PA1, the volumetric percentage varies in a narrow range of 14.5–15.5% as the material density rises from 100 to 2300 kg m^{-3}; for CO at PA2, the volumetric percentage rises from 12 to 14% as the material density increases from 100 to 600 kg m^{-3}, but only small change follows when the density is further increased; for CO at PA3, the trend of change is similar to the situation at PA2, except that the level is around 1.2% lower on the whole.

In general, the CH_4 concentration in the flue gases exiting the bed top increases with increase in the fuel material density, especially when the density is below 800 kg m^{-3}.

H_2 concentration at the bed top only shows a minor rise as the material density increases from the minimum to the maximum.

Fig. 5(d) presents the maximum solid temperature inside the bed as the fuel material density increases. Generally, the maximum solid temperature increases when the fuel material has a higher density. The temperature with the heaviest fuel is around 80 K higher than that with the lightest fuel at the same primary air velocity.

3.4. Effect of bed porosity

Bed porosity depends on a number of factors, including particle size distribution, particle shape, shaking or pressing of the bed, etc. A bed with a low porosity is called a compact bed and a bed with a high porosity is called a loose bed. In this section, the initial bed porosity is artificially changed while keeping all the other bed parameters the same. The porosity covers a range of 0.35–0.75.

Fig. 6(a) demonstrates the effect of bed porosity on the burning rate of the bed. It is seen that the effect of bed porosity depends on the level of primary air velocity. At low primary air velocities (PA1 and PA2), the general trend is decreasing burning rate as the bed porosity increases, though in some ranges the burning rate may maintain a more or less constant level (porosity 0.5–0.65 for PA1 and 0.65 onwards for PA2). At increased primary air velocity (PA3), the maximum burning rate is obtained between bed porosity of 0.45–0.55 and either a looser or denser bed would results in a lower burning rate. However, similar to the situation of PA2, the burning rate keeps constant as the bed porosity increases beyond 0.65.

Fig. 6(b) demonstrates the combustion stoichiometry against the initial bed porosity. Generally, the air-to-fuel stoichiometric ratio increases as the bed porosity increases. But the air-to-fuel ratio keeps constant in some part along the range, i.e. bed porosity from 0.5 to 0.65 for PA1 and from 0.65 onwards for PA2 and PA3.

Fig. 6(c) shows the bed-top gas composition as a function of bed porosity. For CO at PA1, very little change in its level is shown for the whole range of porosity variation; for CO at PA2, the volumetric level in the flue gases exiting the bed top falls in the range of 0.45–0.6 of the bed porosity, otherwise, it keeps a constant value; for CO at PA3,

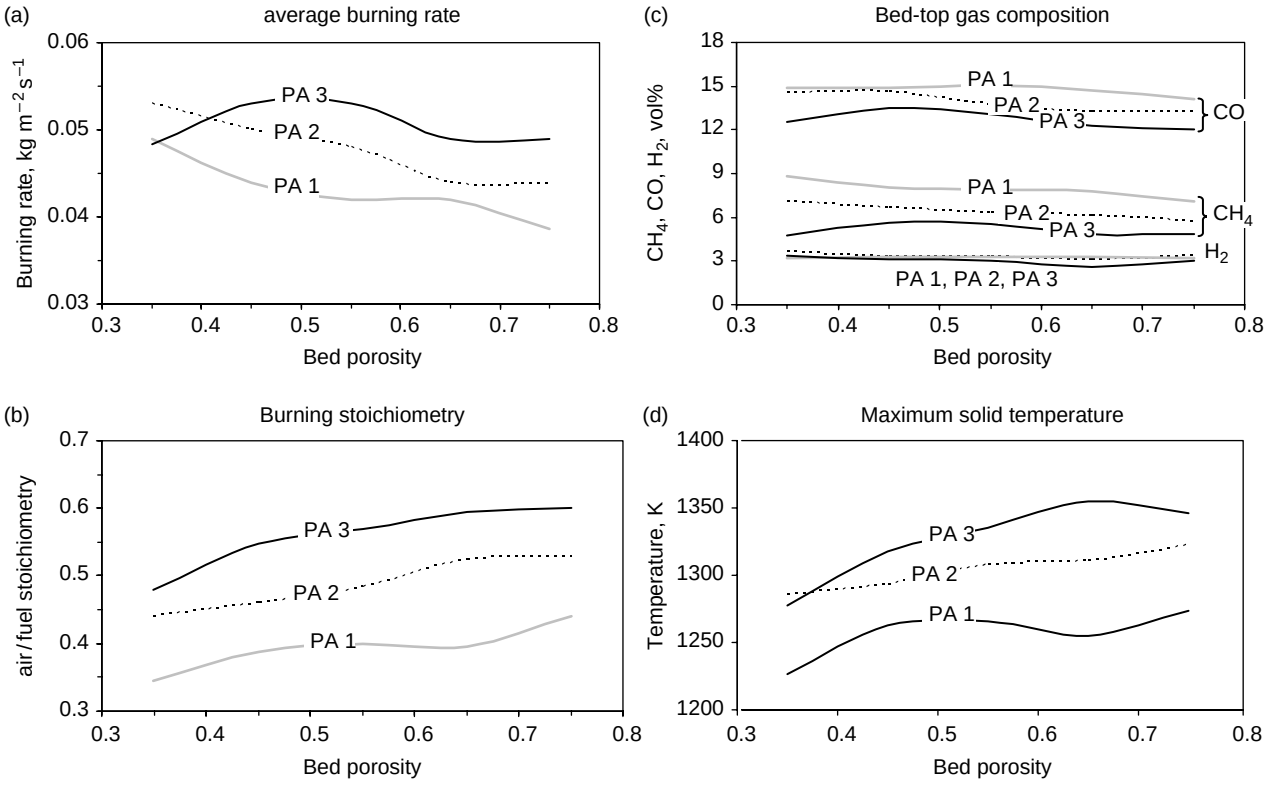

Fig. 6. Effect of bed porosity: (a) average burning rate; (b) combustion stoichiometry; (c) gas composition at the bed top; (d) maximum solid temperature.

the maximum level is obtained around a bed porosity of 0.45 and either a looser or denser bed results in a lower CO concentration at the bed top.

For CH_4 at PA1 and PA2, the general trend is reducing concentration level as the bed porosity increases; for CH_4 at PA3, the maximum level is obtained around the bed porosity of 0.5.

It is also seen that the H_2 concentration is not affected by either the bed porosity or the primary air velocity.

Fig. 6(d) demonstrates the maximum solid temperature against porosity variation. The pattern of variation depends on the primary air velocity. At the low air velocity of PA1, the maximum solid temperature rises as the bed porosity rises from 0.35 to 0.45, but keeps constant from 0.45 to 0.55, falls from 0.55 to 0.65 and then rises again from 0.65 onwards. At PA2, however, a continuous increase in the solid temperature is obtained as the bed porosity increases from the minimum to the maximum. For the situation of PA3, the solid temperature increases with increasing bed porosity until the porosity reaches 0.65, followed then by a fall in the maximum solid temperature as the bed porosity further increases.

4. Discussion and validation against experiments

The effect of moisture content in fuel and the fuel devolatilisation rate on packed-bed solid combustion has been studied earlier by Yang et al. [1,5]. The previous studies have shown that moisture content in fuel has a significant effect on the fuel burning and a very dry fuel can burn up to four times faster than does a very wet fuel. These experimental studies also showed that the kinetic rate of fuel devolatilisation affects the ignition time at high fuel-moisture levels but the effect was less noticeable for dry fuels. For the mass loss rate after the fuel ignition, the kinetic rate of fuel devolatilisation had the opposite effect, i.e. the mass loss rate is only significantly affected by fuel devolatilisation for dry fuels.

The current investigation contributes to the expansion of those previous studies by including more parameters. There are also two aspects different from previous studies: (1) the burning rate presented in this work is the averaged value over the whole combustion period, including ignition, volatile release and final char burnout, while most of the previous works [1–6] presented the burning rate as the gradient of an assumed linear section on the mass-loss curve, which excludes the initial ignition and final char burnout stages and does not reflect the whole combustion process; (2) the maximum solid temperature in the bed is now presented which differs from the traditionally measured maximum flame temperature. The latter cannot distinguish between the gas phase and the solid phase and the solid temperature was rarely addressed before. The mathematical model adopted in this work solves both the gaseous and solid temperature.

The following sections present an interpretation of the results obtained in the current work, and experimental data are presented for comparison wherever this is possible.

4.1. The effect of biomass LCV

The variation in LCV was achieved by varying the mass ratio of combustible elements (C and H) to the oxygen (O) in the fuel, so the effect of LCV is mainly through the change in air-to-fuel stoichiometry as illustrated in Fig. 3(b). In the range of primary air velocity of interest (0.1–0.23 kg m^{-2} s^{-1}), all the combustion of the investigated fuels occurs at the fuel-rich side and an increase in LCV makes the combustion more fuel-rich and hence the solid temperature in the flame front would decrease (Fig. 3(d)) and the CO and H_2 concentrations in the bed increase (Fig. 3(c)). This explains the insensitivity of the burning rate to the increase in LCV at low primary air velocity (0.1 kg m^{-2} s^{-1}). On the other hand, an increase in LCV results in locally stoichiometric combustion of the released volatile fuels occurring earlier in the flame front and nearer to the moisture evaporation front. The local solid temperature would be enhanced in the region of moisture evaporation and early devolatilisation and the rates of these two processes subsequently increase. This factor becomes dominant at higher primary air velocities where a positive relationship between LCV and the burning rate is more obvious (Fig. 3(a)).

The H_2 concentration in the flue gases exiting the bed top depends on the balance of H_2 production and consumption. The H_2 concentration is rather insensitive to the variation in primary air velocity because the production and consumption of H_2 keep more or less in balance as the primary air flow rate varies. The decrease in H_2 concentration at high LCV can be explained by incomplete oxidisation of CH_4 producing CO and H_2 as the burning goes fuel-richer on the whole.

4.2. The effect of particle size

Particle size affects the combustion processes in the bed in four different aspects. First is the two-phase heat and mass transfer between the gas and solid. These convective processes occur at the particle external surfaces and the rates are approximately inversely proportional to the particle diameter. Therefore, particles of a smaller size can enhance the moisture evaporation and char burning rates in the bed. On the other hand, the hot solids may be cooled down by the fresh primary air flow which enters the bed at room temperature.

The second effect is on the radiation heat transfer where the bed absorption of radiation flux is inversely proportional to particle diameter. This means that a bed of smaller particles absorbs radiation more quickly. But the radiation flux, on the other hand, is less absorbed by a packing of larger particles and hence penetrates a longer distance in the bed. This can produce a thicker flame front in the bed and affects the temperature and gas concentration profiles as a consequence.

The third effect is on the turbulent dispersion of energy and gas species in the packed bed. Both thermal and fluid dispersion coefficients are proportional to particle diameter. Larger particles produce larger-scale turbulence in the local bed structure and facilitate the cross-flow and inflow mixing in the gas phase. As a result, the reaction zone in the bed can be thicker for larger particles and thinner for smaller particles.

The fourth effect is on the burning rate of volatile gaseous fuel both in the voids of the bed and in the immediate area above the bed. The process is basically diffusion-controlled. As indicated in the equation summary (Table 2), the mixing rate of the fuel gases with air flow from under the grate is a function of particle size and small particles produce a higher rate (the other conditions being the same) and hence higher combustion intensity in the gas phase.

The obtained results shown in Fig. 4 are just the balanced results of the above factors. Generally, larger particles produce a slower burning rate and lower concentration of CO and CH_4 at the bed top. But H_2 concentration has the opposite trend, i.e. increasing particle size producing a higher H_2 level in the flue gases exiting the bed. This is because the oxidization rate of H_2 decreases with larger particle sizes.

The numerical results for the effect of particle size have been validated against experiments as shown in Fig. 7 for the mass-loss history. Four sizes of pinewood cubes were fired in a stationary packed-bed with an initial height of around 400 mm and primary air velocity of 0.1 kg m^{-2} s^{-1} at an inlet temperature of 300 K (Part I). The bed was ignited at the top by an over-fire pilot gas burner and the primary air was supplied to the bed through the grate at the bottom of the bed. The model calculations generally match the measurements and accurately predict the trend as particle size increases. Both the predictions and

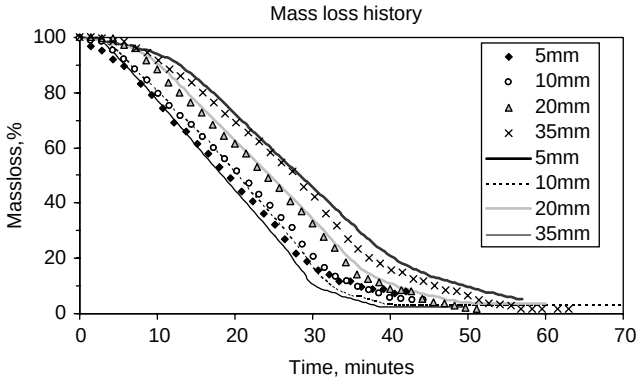

Fig. 7. Particle size effect—mass loss history in a stationary packed bed. Line: model prediction; symbols: measurements of this work (fuel: pinewood; primary air velocity: 0.1 kg m^{-2} s^{-1} at 20 °C)

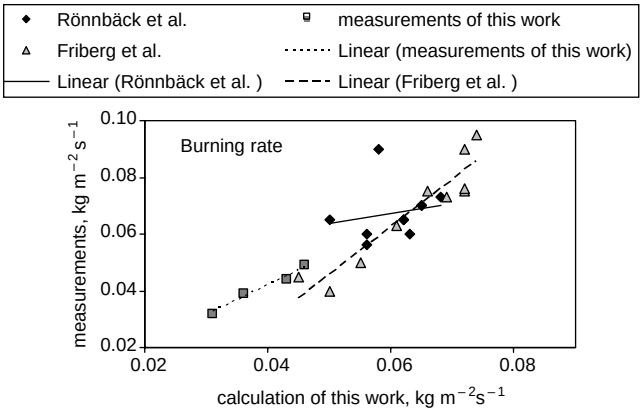

Fig. 8. Particle size effect—comparison of the model calculations of the burning rate to measurements from different sources. Symbols represent the measurements and lines represent the correlation between model calculations and the measurements.

measurements show the three periods in the pinewood combustion, the initial ignition stage followed by the constant combustion stage and the final char-burnout. The rate of the latter slows down as the combustion approaches completion.

The results obtained in this work are consistent with the measurements of Friberg and Blasiak [8] which demonstrated decreasing average burning rate as particles size increased. As mentioned above, Peters [7] reported the maximum ignition rate was obtained at 15 mm in the size range of 5–25 mm where the 5 mm particles produced no flame because the bed could not be ignited at the tested air velocity. Contrary to other researchers' finding, Rönnbäck et al. [6] reported increased ignition speed for larger particles in the size range of 8–34 mm.

Fig. 8 makes a comparison between the model calculations and the measurements of the burning rate from both the current work and other researchers. When compared to the measurements of this work, the average burning rate is used and when compared to the measurements from literature, the burning rate in the constant stage or the maximum rate is used. The correlation lines between the calculations and measurements are also drawn. The R^2 value of those correlations is 0.98 between the calculations and the measurements of this work, 0.88 between the calculations and the measurements of Friberg and Blasiak [8] and 0.05 for between the calculations and the measurements of Rönnbäck et al. [6]. The poor agreement between the calculations and the results of Rönnbäck et al. is possibly due to the particle shape effect (wood cylinders were used) which has not been included into this study and needs to be investigated further. The measurements reported by Peters [7] cannot be directly compared with the calculations because the fuels used in the measurements might have much higher moisture content, but the general trend is in line with the current calculations if the moisture effect is taken into account.

4.3. The effect of material density

For fuels of heavy material, more combustible mass is packed in a smaller volume and the fuel material density mainly affects the reaction zone thickness. Denser material tends to produce a thinner reaction zone, which reduces the residence time of the reacting gases. More heat is also required to heat up a specific volume of bed to the ignition temperature. Light material, on the other hand, tends to lose temperature easily by radiation as it has a smaller heat capacity per unit of volume. The combustion stoichiometry determines the bed temperature and a denser material has a higher maximum bed temperature as it has a less fuel-rich combustion condition. The concentrations of CO, CH_4 and H_2 in the flue gases exiting from the bed top increase as the material density increases due to the shorter residence time of the gases.

4.4. The effect of bed porosity

Bigger voids in the bed facilitate radiation penetration in the bed, but reduce mixing between the released volatile gases and the under-grate air flow and hence the gas-phase burning intensity. Void fraction also changes the gas-phase

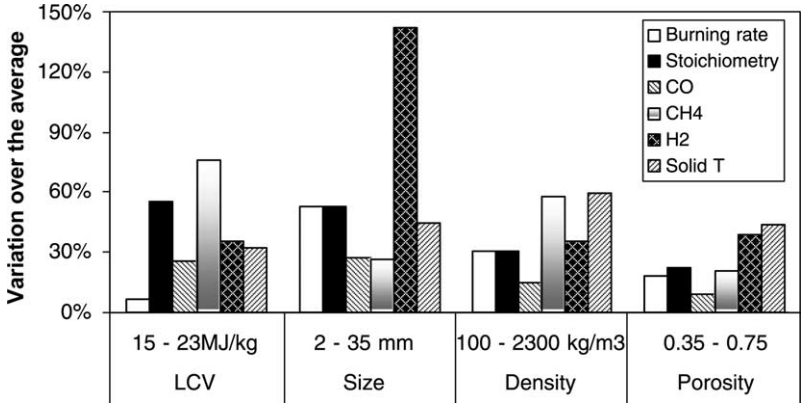

Fig. 9. Summary of the effects of different fuel properties.

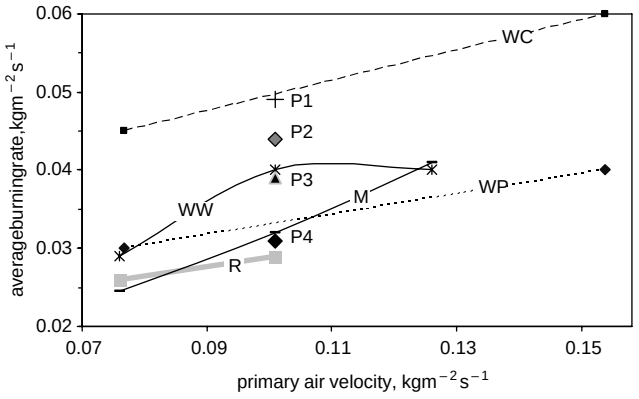

Fig. 10. Experimental measurements of burning rate for different type of fuels. Friberg and Blasiak [8]: WP: wood pellets (L=30 mm, ∅=6 mm); WW: wood chips (L=4–30 mm, ∅=2–5 mm). This work: R: residual deduced fuel (L=30–50 mm, ∅=7 mm); M: miscanthus pellets (L=5–8 mm, ∅=3 mm); WW: willow chips (L=10–40 mm, ∅=4–8 mm); P1: pinewood cubes (5 mm); P2: pinewood cubes (10 mm); P3: pinewood cubes (20 mm); P4: pinewood cubes (35 mm).

residence time in the bed as the bed becomes loose and bulky. At low air velocity, gas-phase mixing is the controlling factor, and the higher the bed porosity, the lower the gas-phase combustion rate; at high air velocity, radiation penetration as well as residence time of gases become important and the best results are around 0.45–0.55. But for a very compact bed and a very light material, local fluidisation or channelling can occur which will alter the trend. A slight decrease in bed-top CO and CH_4 at high bed porosity is the balanced result between reduced mass-loss rate and the slower reaction (mixing) rate of those combustible gases with primary air.

A summary of the effects of different fuel properties is illustrated in Fig. 9. It shows the relative variations in percentage of the six burning parameters (average burning rate, combustion stoichiometry, CO, CH_4 and H_2 in the flue gases exiting the bed top and the maximum solid temperature) around their average values as the four investigated fuel properties are varied over their designated ranges, respectively. It is seen that for average burning rate, the particle size has the greatest effect followed by fuel density, while LCV has the smallest effect; the combustion stoichiometry is most affected by both LCV and fuel size, while bed porosity has the smallest influence and a similar conclusion is obtained for CO; for CH_4, fuel LCV and material density are found to have the greatest effect and bed porosity has the least; for H_2, fuel size has a remarkably strong effect compared to the other three fuel properties; for the solid temperature, all the four properties have a noticeable effect with material density having the greatest.

4.5. Application to practical systems

The above results obtained in this work can be used to explain or understand the performance of real systems under similar conditions. Fig. 10 shows the experimental measurements of the burning rate with nine different fuels from both this work and Friberg and Blasiak [8]. The fuels included chips and pellets of a mixture of pine and spruce, pinewood cubes, willow chips, miscanthus pellets and refuse derived fuel (RDF) pellets. For pinewood cubes, the size ranged from 5 to 35 mm and a fixed primary air velocity was employed. For fuel LCV, the order from the lowest to highest is miscathus (16 MJ kg^{-1}), wood mixture (17 MJ kg^{-1}), willow wood (18 MJ kg^{-1}), pinewood (19 MJ kg^{-1}) and RDF (21 MJ kg^{-1}). For bed porosity, all the fuels are estimated to be the same around 0.55–0.6. For particle size and material density, the orders are shown in Table 3.

The general trend obtained from calculations show that higher LCV, smaller particle sizes and lower material density all favour a higher burning rate (see Figs. 3(a), 4(a) and 5(a)) and lower bed porosity favours a higher burning rate at low primary air velocity but the optimum is reached around 0.5 when primary air flow rate is high (see Fig. 6(a)). The calculations also show that among the above four fuel properties, particle size has the strongest effect, followed by material density. Porosity is the second least significant and LCV has the least effect. So roughly, the burning rate is

Table 3
Burning rate order of nine different fuels deduced from calculation results

Fuel type	Size	Size order	Density (est.) (kg m^{-3})	Density order	Deduced burning rate order
Miscanthus pellets	∅=3 mm, L=5–8 mm	1	1650	2	5
Wood mixture chips	∅=2–5 mm, L=4–30 mm	2	700	1	1
Pinewood cubes	5 mm×5 mm×5 mm	2	700	1	1
Pinewood cubes	10 m×10 mm×10 mm	3	700	1	2
Willow chips	∅=4–8 mm, L=10–40 mm	4	450	1	3
Wood mixture pellets	∅=6 mm, L=30 mm	5	1650	2	6
RDF	∅=7 mm, L=30–50 mm	6	1800	3	8
Pinewood cubes	20 mm×20 mm×20 mm	7	700	1	4
Pinewood cubes	35 mm×35 mm×35 mm	8	700	1	7

Note that (1) the order is from small to large for size and density and high to low for burning rate; (2) densities of 450 and 700 kg m^{-3} are considered at the same level from the results shown in Fig. 5(a).

determined firstly by the fuel size and secondly by the material density.

Based on the above theoretical conclusion, Table 3 shows the deduced burning rate order of the nine different fuels. Wood mixture chips (symbol WC) and the pinewood cubes of 5 mm (symbol P1) come to the top because these two fuels have the smallest sizes (apart from miscanthus pellets) and the lowest material density. Miscanthus pellets are the smallest but have a very high density and the obtained burning rate is listed number 5 of the nine fuels. The RDF pellets come to the bottom of the list due to their highest material density and a relatively large size. For other fuels, the level of the burning rate depends on the combination of particle size and material density.

The deduced results in Table 3 match the experimental results shown in Fig. 10 and demonstrate the validity of the theoretical calculations. This provides great help in understanding and explaining the performance of practical systems. It also helps designers as well researchers predict the rough burning characteristics of a new fuel. Nevertheless, the conclusions in this study are still qualitative and care must be taken when using them in very different situations. The current work also did not carry out a multivariable study where all the concerned parameters are varied at the same time. This would result in huge computation tasks that are beyond the ability of current human and machine resources.

5. Conclusions

A numerical method has been employed to simulate the effects of the four fuel properties on the burning characteristics of biomass in packed bed systems. The major conclusions are summarised in the following:

(1) average burning rate is mostly influenced by fuel size and smaller fuels result in higher combustion rate due to increased reacting surface area and enhanced gas-phase mixing in the bed;
(2) combustion stoichiometry is equally influenced by fuel LCV and size as a consequence of variation in burning rate as well as the mass ratio of combustible elements (C and H) to the oxygen (O) in the fuel; higher LCV, smaller particle size, lower material density and a more compact bed all favour a more fuel-rich combustion as a general trend;
(3) for the solid-phase temperature, material density has the strongest influence and a denser material has a higher maximum bed temperature as it results in a less fuel-rich combustion condition;
(4) for CO concentration in the flue gases exiting the bed top, both LCV and particle size have the strongest effect due to change in combustion stoichiometry; higher LCV and smaller particle size result in high CO;
(5) for CH_4 concentration in the flue gases exiting the bed top, both LCV and material density have the dominant influence; denser material tends to produce a thinner reaction region and reduce the residence time of the reacting gases so that less CH_4 is burnt;
(6) particle size has the greatest effect on the H_2 concentration in the bed; bsigger particles produce a higher H_2 level in the flue gases exiting the bed top; this is because the oxidization rate of H_2 deceases with larger particle sizes.
(7) calculated results agreed qualitatively with experiments and explain satisfactorily the observed performance of nine different fuels.

Acknowledgements

The authors thank the UK Engineering and Physical Sciences Research Council (EPSRC) for the financial support of this project.

References

[1] Yang YB, Yamauchi H, Sharifi VN, Swithenbank J. Effect of moisture on the combustion of biomass and simulated solid waste in a packed bed. J Inst Energy 2003;76:105–15.
[2] Yang YB, Swithenbank J, Sharifi VN. Effect of air flow rate and fuel moisture on the burning behaviours of biomass and simulated solid waste in a packed bed. Fuel 2004;83:1553–62.
[3] Thunman H, Leckner B. Ignition and propagation of a reaction front in cross-current bed combustion of wet biofuels. Fuel 2001;80:473–81.
[4] Gort, R. On the propagation of a reaction front in a packed bed: thermal conversion of municipal waste and biomass. Academic Dissertation, University of Twente; 1995.
[5] Yang YB, Sharifi VN, Swithenbank J. Effects of fuel devolatilisation on the combustion of wood chips and incineration of simulated municipal solid wastes in a packed bed. Fuel 2003;82:2205–21.
[6] Rönnbäck M, Axell M, Gustavsson L, Thunman H, Leckner Bo. Combustion processes in a biomass fuel bed-experimental results. Progress in Thermochemical Biomass Conversion, Tyrol, Austria; 17–22 September, 2000.
[7] Peters B. Thermal conversion of solid fuels. Southampton: WIT Press; 2003.
[8] Friberg R, Blasiak W. Measurements of mass flux and stoichiometry of conversion gas from three different wood fuels as function of volume flux of primary air in packed bed combustion. Biomass Bioenergy 2002;23:189–208.
[9] Yang YB, Goh YR, Zakaria R, Nasserzadeh V, Swithenbank J. Mathematical modeling of MSW incineration on a travelling bed. Waste Mgmt 2002;22:369–80.
[10] Thunman H. Principles and models of solid fuel combustion. PhD Thesis. Chalmers University of Technology, Göteborg, Swenden; 2001.
[11] Badzioch S, Hawksley PGW, Peter CW. Kinetics of thermal decomposition of pulverized coal particles. Ind Eng Chem Process Des Develop 1970;9:521–30.
[12] Alves SS, Figueiredo JL. Pyrolysis kinetics of lignocellulosic materials by multistage isothermal thermo-gravimetry. J Analyt Appl Pyrolysis 1988;13:123–34.

[13] Smoot LD, Pratt DT. Pulverised-coal combustion and gasification: theory and applications for continuous flow processes. London: Plenum Press; 1979.
[14] Gosman AD, Lockwood FC. Incorporation of a flux model for radiation into a finite-difference procedure for surface calculations. Proceedings of the 14th Symposium (International) on Combustion. Pittsburgh, PA: The Combustion Institute; 1972 p. 661–71.
[15] Goh YG, Yang YB, Zakaria R, Siddall RG, Nasserzadeh V, Swithenbank J. Development of an incinerator bed model for municipal solid waste incineration. Combust Sci Technol 2001;162: 37–58.
[16] Siminski VJ, Wright FJ, Edelman RB, Economos C, Fortune OF. Research on methods of improving the combustion characteristics of liquid hydrocarbon fuels, AFAPL TR 72-74, vols. I and II, Air Force Aeropropulsion Laboratory, Wright Patterson Air Force Base, OH; 1972.
[17] Howard JB, William GC, Fine DH. Kinetics of carbon monoxide oxidation in postflame gases. Proceedings of the 14th Symposium (International) on Combustion. Pittsburgh, PA: The Combustion Institute; 1973 p. 975–86.
[18] Hautman AN, Dryer FL, Schlug KP, Glassman I. A multiple-step overall kinetic mechanism for the oxidation of hydrocarbons. Combust Sci Technol 1981;25:219.
[19] Arther JA. Reactions between carbon and oxygen. Trans Faraday Soc 1951;47:64–178.
[20] Gray D, Cogoli JG, Essenhigh RH. Problems in pulverised coal and char combustion. Adv Chem Ser 1974;131:72–91.
[21] Field MA. Rate of combustion of size-graded fractions of char from a low rank coal between 1200 and 2000 K. Combust Flame 1969;13: 237–52.
[22] Peters B. A detailed model for devolatilization and combustion of waste material in packed beds. Proceedings of the Third European Conference on Industrial Furnaces and Boilers (INFUB), Lisbon, Portugal; 18–21 April, 1995.
[23] Wakao N, Kaguei S. Heat and mass transfer in packed beds. London: Gordon & Breach; 1982.
[24] Shin D, Choi S. The combustion of simulated waste particles in a bed. Combust Flame 2000;121:167–80.